Alluvial Sapphires from Montana: Inclusions, Geochemistry, and Indications of a Metasomatic Origin

J.C. (Hanco) Zwaan, Eric Buter, Regina Mertz-Kraus, and Robert E. Kane

Although the source rocks of alluvial sapphires in Montana have never been discovered, inclusions and geochemistry of material from this location may give clues to their original source. Mineral inclusions in alluvial Montana sapphires, mainly from Rock Creek, were identified and compared with existing data. Topaz was a remarkable find in one of these samples; other newly identified mineral inclusions in Montana sapphire were allanite, anatase, chalcopyrite, and monazite. Together with the presence of calcium-rich plagioclase, alkali-feldspar, apatite, barite, phlogopite, a pyrochlore-group mineral previously called uranpyrochlore, and chromite/spinel, these inclusions may reflect a metasomatic origin for the sapphires. This is supported by their chemical composition, which largely coincides with sapphires of plumasitic/metasomatic origin. The secondary Montana sapphires analyzed in this study are characterized by mean values of Fe (4686 ppmw), Ti (58 ppmw), Ga (51 ppmw), Mg (35 ppmw), and Cr (21 ppmw). Fe-Mg-Ga ratios help to distinguish them from sapphires with overlapping properties, such as those from Umba, Tanzania, and Rio Mayo, Colombia.

While Yogo Gulch is Montana's only primary sapphire deposit, alluvial deposits occur near Philipsburg (Rock Creek), Deer Lodge (Dry Cottonwood Creek), and Helena (Missouri River; figure 1). Eldorado Bar is the largest and best known of the approximately 14-mile-long Missouri River deposits. Other historically mined sapphire deposits—in gravel bars on both sides of the river, as well as the riverbed itself—are American Bar, Dana Bar, Metropolitan Bar, Spokane Bar, French Bar, Magpie Gulch, and Emerald Bar.

Figure 1. Locations of sapphire deposits in the U.S. state of Montana. Yogo Gulch is the only primary deposit, while Rock Creek is the most important alluvial deposit.

Rock Creek, popularly known as Gem Mountain, is the most important of Montana's secondary deposits (Kane, 2004, 2008; Berg, 2014). Huge quantities of sapphire have been produced in this area. Between 1906 and 1923, 190 million carats were shipped from Rock Creek, and during the mid-1990s more than 3.5 million carats were produced (Kane, 2004). Between the 1920s and 1990s there was very little to no production, if any. Production stopped in the 1930s, mainly because of fierce competition from synthetic sapphires used in the watch industry. By the 1970s the public could screen gravel for sapphires. Despite favorable sampling results obtained from a 3,700-cubic-yard sample between 1974 and 1976, the pale-colored material was not considered marketable. Production resumed only after it was discovered that heat treatment induced appealing colors (compare

See end of article for About the Authors and Acknowledgments.
Gems & Gemology, Vol. 51, No. 4, pp. 370–391,
http://dx.doi.org/10.5741/GEMS.51.4.370.

Figure 2. Montana sapphires occur at three commercial secondary deposits: Rock Creek, Dry Cottonwood Creek, and the Missouri River area. These rough and faceted Rock Creek stones show the range of permanent colors after routine heat treatment without the addition of chemicals. The largest faceted gem weighs 0.43 ct, and the largest rough stone weighs 1.86 ct. Courtesy of Fine Gems International, © Robert E. Kane.

Berg, 2014). Yet the source and origin of these alluvial deposits remains unclear, despite more than 100 years of searching (e.g., Pratt, 1906; Clabaugh, 1952; Garland, 2002; Berg, 2011).

To avoid confusion within the gem trade, specific nomenclature is used to differentiate Montana sapphires by rarity, the nature of the deposit (primary versus secondary), and the application of heat treatment (a common practice in enhancing the colors of the alluvial sapphires). The sapphires from the primary deposit at Yogo Gulch, routinely called "Yogo sapphires," are unique in that they have a very uniform, intense color and thus do not require heating. The sapphires that come from the secondary deposits of the Missouri River, Dry Cottonwood Creek, and Rock Creek are simply referred to as "Montana sapphires" (figure 2). Throughout the present article, the authors follow this convention.

The geology of western Montana is dominated by Cenozoic episodes of basin development and deformation (resulting in a fold-thrust belt and *foreland basin**), in response to subduction of the Pacific plate

*Italicized geochemical terms are defined in the glossary on p. 389.

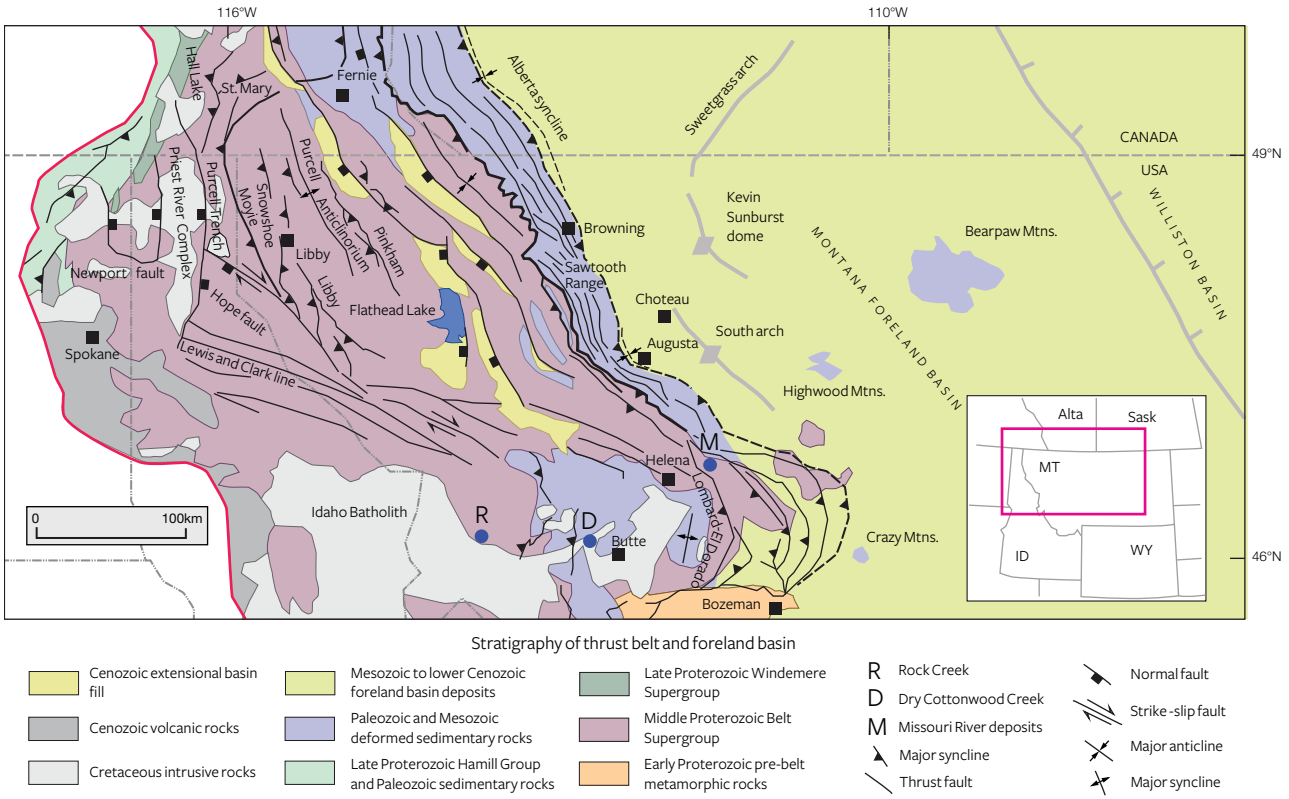

Figure 3. Simplified regional tectonic map of the fold-thrust belt and foreland basin of northwestern Montana (MT) and adjacent areas (Idaho – ID, Wyoming – WY, Alberta – Alta., and Saskatchewan – Sask.) From Fuentes et al. (2012).

along the western continental margin (figure 3; Garland, 2002; Fuentes et al., 2012). The geological framework has a foundation in the Archean and Proterozoic development of the North American continent. The Proterozoic basin formed a large trough trending northwest, and most of the sediments accumulated in the basin from 1470 to 1400 Ma at a relatively rapid rate (Evans et al., 2000). Locally, Paleozoic and Mesozoic sediments are exposed (though often poorly, as the large sedimentary basins of these periods have mostly been overprinted by Cenozoic tectonics). Large sections of Proterozoic belt sediments uplifted by Cretaceous thrust faulting compose most of the bedrock in the Rock Creek area (Garland, 2002; Fuentes et al., 2012). After an onset of igneous activity during the Late Cretaceous and Paleocene epochs (approximately 80–58 Ma), resulting in the emplacement of the Idaho *batholith* (figure 3), Eocene and younger mafic to ultramafic alkalic, igneous rocks (< 54 Ma) intruded the region. Of these rocks, a lamprophyric ultramafic dike (called ouachitite, a variety of monchiquite, characterized by the abundance of black mica and brown amphibole, olivine, clinopyroxene, analcime) and *hydrothermal breccia* host the Yogo sapphire deposit (e.g., Clabaugh, 1952; Baker, 1992; Baker, 1994; Giuliani et al., 2007). In the Rock Creek area, tertiary sediments and volcanics lie *nonconformably* (with a substantial gap in the geological record) on tilted Proterozoic Belt series sediments (figure 4). Here, the main unit of the Eocene volcanic rocks (approximately 50 Ma) is a porphyritic rhyolite or rhyodacite flow

In Brief

- Mineral inclusions and geochemical features of alluvial Montana sapphires may reflect a metasomatic origin.
- Geochemistry is also useful in differentiating sapphires of Montana origin from sapphires from other localities.
- Fe-Mg-Ga ratios help to distinguish Montana sapphires from material with overlapping properties originating in Umba, Tanzania and Rio Mayo, Colombia.
- Topaz inclusions within sapphire may also indicate a Montana origin.

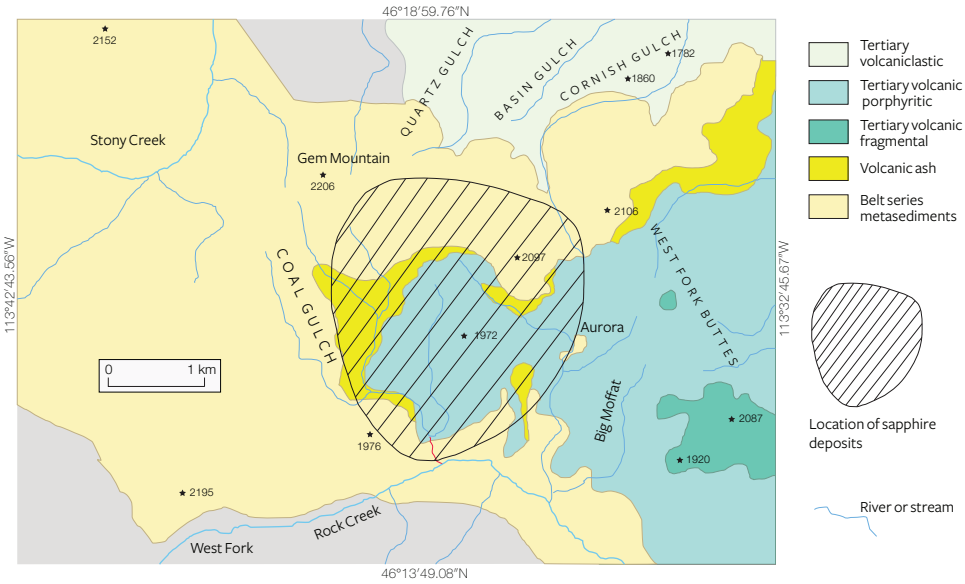

Figure 4. Geological sketch map of the Rock Creek area showing the location of the alluvial sapphire deposits. Modified from Garland (2002).

(Garland, 2002; Berg, 2011, Berg, 2014) or, close by, a felsic lapilli tuff (Berger and Berg, 2006; Berg, 2007).

The Yogo primary sapphire deposit is well characterized. Although several hypotheses have been presented for the origin of these gems, the chemical composition of garnet inclusions strongly supports the idea that the sapphires are xenocrysts, formed in a mantle eclogite and subsequently brought to the surface by lamprophyric magma (Cade and Groat, 2006; Giuliani et al., 2007; also compare Baker, 1994; Mychaluk, 1995). The sub-euhedral to euhedral pale reddish orange garnets were Cr-poor (0.02 wt.%), low in TiO_2 (0.12 wt.%) and Na_2O (0.02 wt.%), and had average values of MgO (10.7 wt.%), FeO (14.0 wt.%), and CaO (11.2 wt.%) (Cade and Groat, 2006). This indicates that the garnet inclusions were formed in the mantle in group II eclogite, according to Schulze (2003), and that the Yogo sapphires are xenocrysts in the melt, also originating from the mantle.

In contrast, the source and origin of the alluvial deposits are highly enigmatic. The Pleistocene in most of North America was marked by several periods of glaciation, and Garland (2002) suggested that the distribution of the alluvial sapphires in the Rock Creek deposit is due to a post-glacial redistribution of a previously existing paleoplacer of the Pliocene age. The erosion of the paleoplacer resulted in concentrations of sapphires through increased fluvial activity. Garland (2002) further advocated a metamorphic origin, *sensu stricto*, at mid-crustal levels, with an inferred minimum temperature of corundum formation at 600–700°C (deducted from hercynite inclusions in Rock Creek sapphires), with magnetite exsolved around the contact. Based on the assumption of equilibrium of the corundum-anorthite-clinozoisite-muscovite assemblage, and working with the composition of a garnet inclusion, $Grs_{10}Alm_{42}Pyr_{47}$, pressure-temperature (P-T) diagrams indicate approximate formation conditions of 13 kbar and 720°C at $aH_2O = 1$, and 9 kbar and 580°C at $aH_2O = 0.5$. The dominance of CO_2 in the fluid inclusions indicates a CO_2-rich and/or high-grade metamorphic crystal growth environment. These formation conditions suggest a crystallization depth of approximately 30 km.

Berg (2011) proposed that in the Rock Creek area, the rhyolitic volcanic rocks are the bedrock source—based on the concentration of sapphires in alluvial deposits proximal to or surrounded by rhyolite, the occurrence of sapphires with attached rhyolite, and the lack of fractures and abrasion—indicating limited fluvial transport. At Silver Bow, a minor alluvial occurrence south of Dry Cottonwood Creek, Berger and Berg (2006) and Berg (2007) distinguished two populations of sapphires, in which pastel sapphires (mainly with shades of green, blue, and yellow) showed signs of resorption at the surface and, in some cases, reaction rims with spinel. Fragments of corundum-bearing biotite-sillimanite schist were also found at Silver Bow. Based on these observations, pastel sapphires were interpreted as xenocrysts of metamorphic origin. Berger and Berg (2006) further argued that dark blue sapphires did not show evidence of resorption or reaction minerals, and postulated them to be magmatic phenocrysts, the source melt of which is represented by a 5 mm fragment of dark blue sapphire–bearing igneous rock, recovered from the debris-flow deposits.

When source rocks of sapphire are largely unidentified, inclusions and chemical composition may give additional clues to their original source and genesis. We identified mineral inclusions, characterized the sapphires chemically, and compared our results with existing data.

MATERIALS AND METHODS

A parcel of approximately 400 faceted sapphires, with a total weight of 702.63 carats, was studied. These samples had been previously removed from the faceted sapphire inventory of the American Gem Corporation (AGC) because of their many large mineral inclusions, which made them ideal for the present study. The samples were mostly brilliant cut, of variable size (mostly between 0.9 and 2.6 ct) and color (see figure 5). Their color ranged from pale to dark blue, yellow to orange, colorless to pale green, and parti-colored (blues and greens with yellow to orange portions). Although most of the parcel was from Rock Creek, a few stones from Dry Cottonwood Creek and the Eldorado Bar deposit on the Missouri River were also included, due to mixing of sapphires from those deposits by the AGC. During the mid-1990s, AGC mined more than 3.5 million carats from Rock Creek and 500,000 carats from Dry Cottonwood Creek. A test mining program at the Eldorado Bar deposit produced several kilograms of rough. All the stones were routinely heat treated.

Figure 5. A selection of alluvial Montana sapphires from this study. These samples weigh between 0.88 and 1.38 ct. The entire parcel ranged from approximately 0.9 and 2.6 ct and weighed 702.63 carats total. Courtesy of Fine Gems International, © Robert E. Kane.

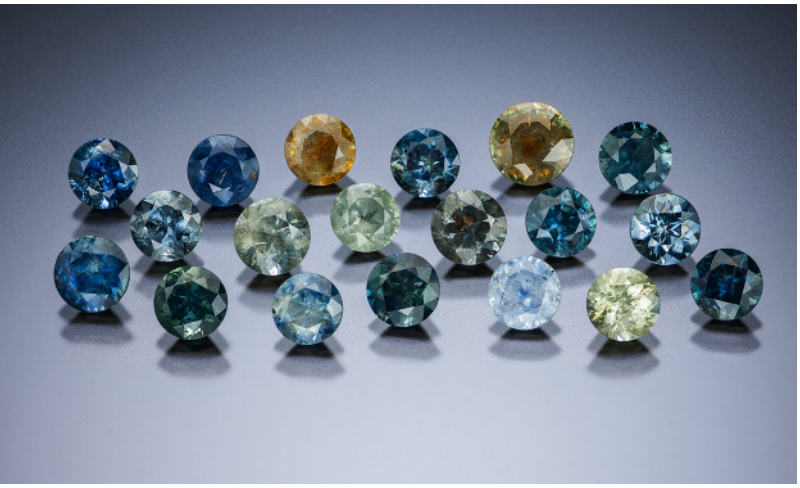

Microscopic Analysis. Internal features were observed with a standard gemological microscope and a Nikon Eclipse E600 POL polarizing microscope. After selecting sapphires that contained recognizable mineral inclusions, we analyzed 98 dark blue samples, along with 18 green and 9 yellow to orange stones, with a Thermo DXR micro-Raman spectrometer using 532 nm laser excitation. Raman spectra were collected at room temperature in confocal mode, which is necessary for analysis of individual inclusions on a micron scale (1–2 µm). A grating of 1800 grooves/mm and a pinhole size of 25 µm, combined with the optical path length, yielded a spectral resolution of 1.0 cm^{-1}. The Raman spectra were interpreted with the help of the RRUFF Raman database of minerals (rruff.info) and other sources (e.g., Wang et al., 2004; Freeman et al., 2008). Depending on the size, position, and orientation of the inclusion analyzed relative to the surface of the host material, the sapphire's Raman peaks at 416 and (rarely) 378 cm^{-1} sometimes appeared in the inclusion's spectrum.

Laser Ablation–Inductively Coupled Plasma–Mass Spectrometry (LA-ICP-MS). LA-ICP-MS was used to determine the trace-element composition of 52 of the faceted alluvial sapphires, which were selected after microscopic analysis. Analyses were performed at the Institute of Geosciences, Johannes Gutenberg University (Mainz, Germany), using an ESI NWR 193 nm Excimer laser with an output wavelength of 193 nm coupled to an Agilent 7500ce quadrupole ICP-MS.

Three spot analyses were performed on each sample. We used a spot size of 100 µm and a pulse repetition rate of 10 Hz. The energy density was about 2.6 J/cm^2. Ablation was carried out under a helium atmosphere, and the sample gas was mixed with Ar before entering the plasma. Background signals were measured for 15 seconds, followed by 60 seconds of ablation and 20 seconds of washout. We used the multi-element synthetic glass NIST SRM 610 for calibration of the element concentrations, applying the preferred values for NIST SRM 610 reported in the GeoReM database (http://georem.mpch-mainz.gwdg.de; Jochum et al., 2005, 2011) to calculate the element concentrations of the samples. We analyzed USGS BCR-2G and NIST SRM 612 at least nine times during each sequence as quality control materials (QCM) to monitor the precision and accuracy of the measurements. A high-purity synthetic corundum sample was analyzed in addition to the unknown samples to validate the measurements. The calibration with NIST SRM 610 yielded a Ca concentration of several hundred ppmw for the

high-purity synthetic corundum, as it did for the unknown samples. Therefore, we assume Ca to be below the detection limit in all of the unknown samples. The measured Ca values are probably due to interference from the corundum matrix ($^{16}O + {}^{27}Al$) on ^{43}Ca (May and Wiedmeyer, 1998).

Glitter 4.4.1 software (www.glitter-gemoc.com) was used for data reduction. Measured isotope intensities were normalized to ^{27}Al, applying an Al_2O_3 content of 100 wt.% for the corundum samples and the values reported in the GeoReM database for the QCM. For most elements, the measured concentrations on the QCM agreed within 15% with the preferred values reported in the GeoReM database (Jochum et al., 2005, 2011). With the QCM, relative standard deviations for the averaged element concentrations determined during the experiment were typically less than 7%. Element/Al ratios were calculated using the element concentrations determined and the assumed Al_2O_3 content of 100 wt.%.

RESULTS

Mineral Inclusions. The sapphire samples were selected for their prominent mineral inclusions, as well as other features such as fissures and an abundance of negative crystals, which often showed characteristic dendritic-like surfaces (figure 6). Rutile was the dominant mineral inclusion identified by Raman spectroscopy. Needles exsolved along the crystal plane directions of corundum were observed in a

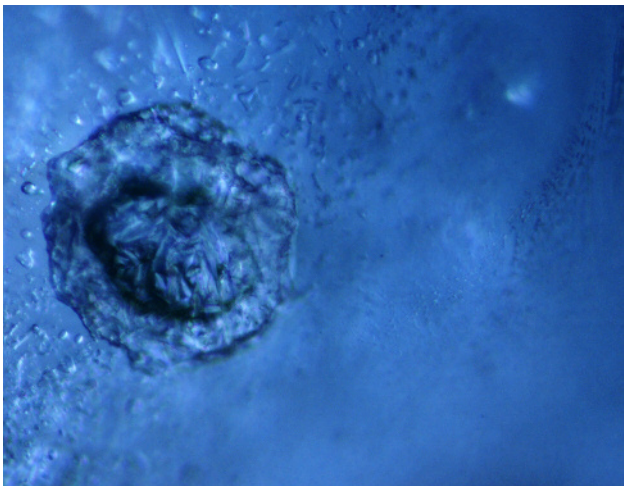

Figure 6. Negative crystals in a blue sapphire showed dendritic surfaces. Photomicrograph by Hanco Zwaan; field of view 0.35 mm.

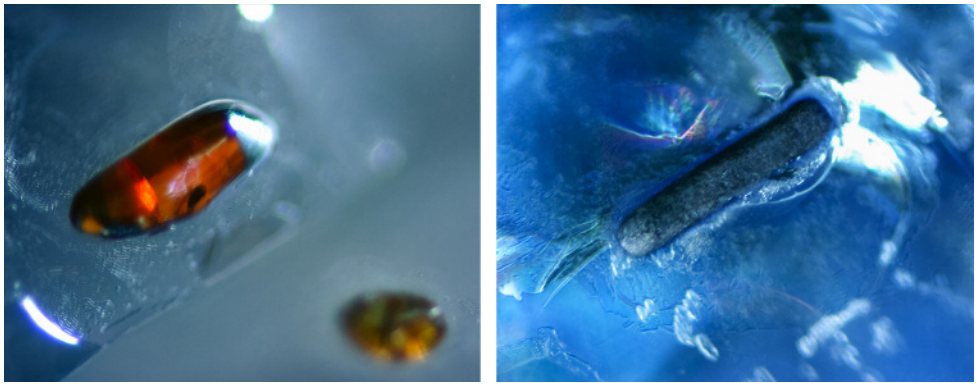

Figure 7. Prismatic and rounded rutile crystals, both orangy brown (left) and black (right), were encountered using a combination of dark-field and oblique illumination. Photomicrographs by Hanco Zwaan; field of view 0.7 mm (left) and 1.4 mm (right).

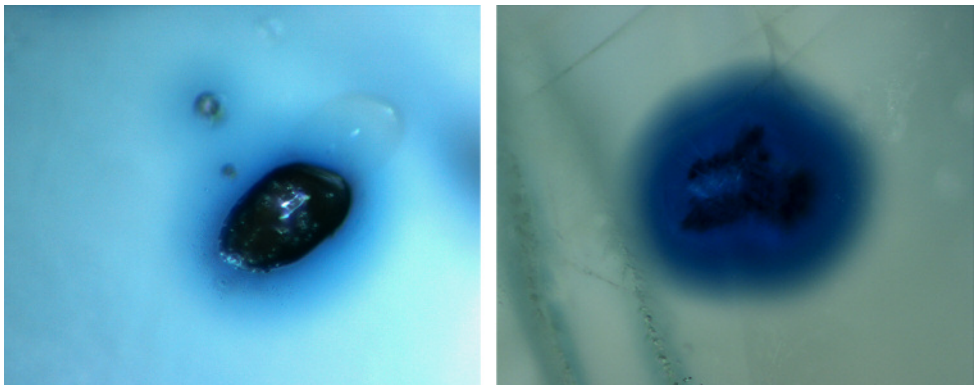

Figure 8. Blue halos were seen around prismatic rutile, but more often around irregularly shaped grains (using transmitted light and oblique illumination on the left and transmitted light on the right). Photomicrographs by Hanco Zwaan; field of view 0.35 mm (left) and 0.7 mm (right).

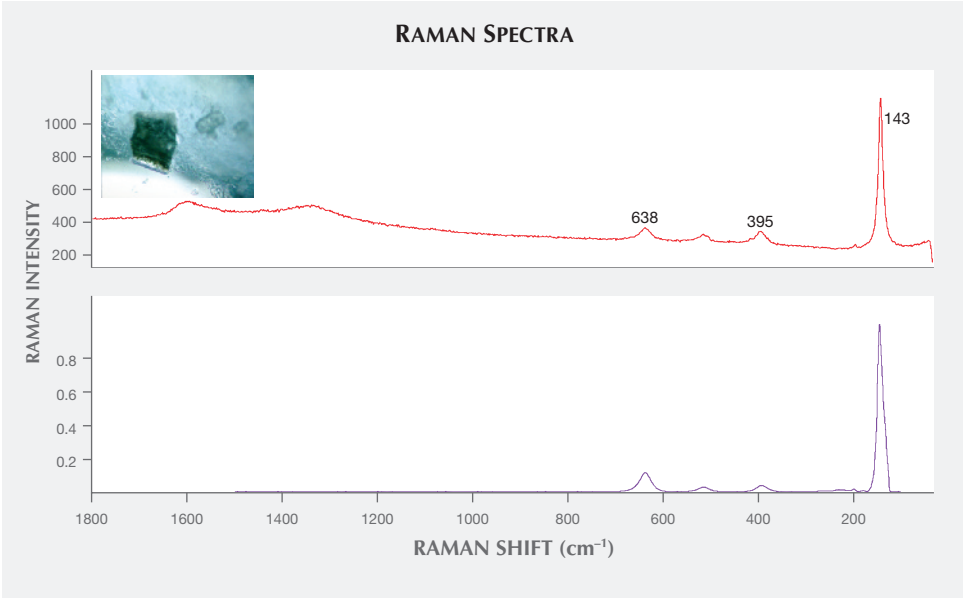

Figure 9. Anatase, another polymorph of TiO_2, is seen here using a combination of oblique and darkfield illumination (inset). The Raman spectrum (top) showed a perfect match with spectra of anatase in the RRUFF database (bottom). Photomicrograph by Hanco Zwaan; field of view 0.7 mm.

number of sapphires, but prismatic and rounded transparent (orangy) brown or black crystals were more common (figure 7), occasionally with a blue halo (figure 8, left). Moreover, we encountered irregularly shaped rutile grains that usually occurred with a blue halo (figure 8, right). Anatase, the relatively rare polymorph of TiO_2, was also found in three sapphires (figure 9).

Ca-rich plagioclase (spectral matches with anorthite and bytownite) and alkali feldspar (with most spectral matches closest to orthoclase) were occasionally encountered. The orientation and prismatic shape of a plagioclase crystal located in the core of a sapphire crystal suggests a protogenetic origin (figure 10). Apart from the spectral matches with the RRUFF database, spectra with bands at 503 and 487 cm^{-1}, with a very weak feature at 460 cm^{-1} (group I) and bands at 282 cm^{-1} and 197 cm^{-1} (figure 11), showed a close match with the anorthite spectra of Freeman et al. (2008). The separation between the main group I bands was approximately 17 cm^{-1}, close to the average of 19.5 cm^{-1} for anorthite and bytownite compositions. For other members of the plagioclase series with an intermediate composition (labradorite, andesine, and oligoclase), the separation between the main group I bands was about 30 cm^{-1}, closer to that of Na-feldspar than Ca-feldspar. Also as in Freeman et al. (2008), the spectra with bands at 512, 480, and 452 cm^{-1} (group I) and bands at 282 and 175 cm^{-1} matched closely with orthoclase, confirming the presence of a potassium-rich feldspar.

Allanite, a black to brown epidote-group mineral with a spectral match closest to allanite-Ce (figure 12), was found in four sapphires. Spectra of the inclusions were similar to those in the RRUFF database for allanite-Ce from Arendal, Norway, and allanite

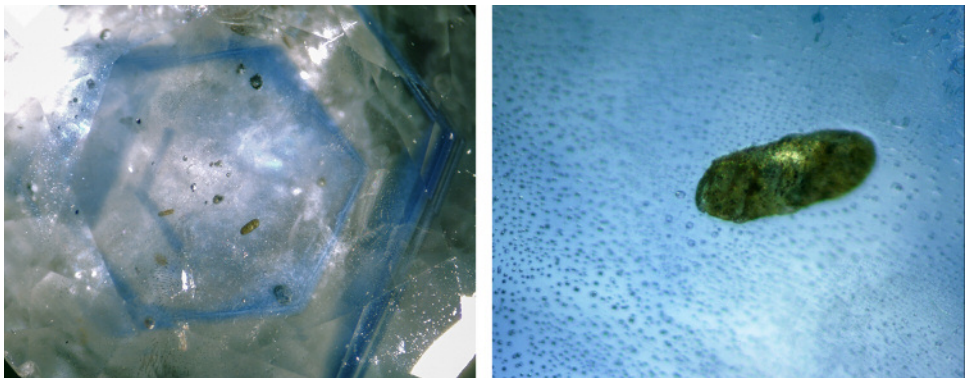

Figure 10. Calcium-rich plagioclase in the core of a sapphire crystal with hexagonal growth zoning. The prismatic shape (enlarged on the right) and orientation suggest a protogenetic origin. Photomicrographs by Hanco Zwaan, using combination oblique and darkfield illumination; field of view 6.4 mm (left) and 0.7 mm (right).

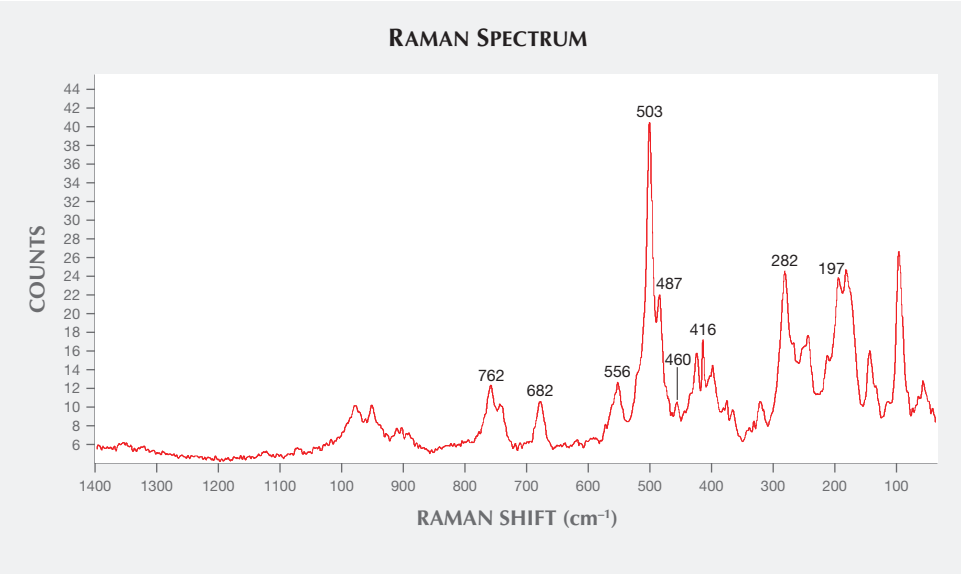

Figure 11. A Raman spectrum of calcium-rich plagioclase, with main peaks at 503 and 487 cm^{-1}, is typical for plagioclase with anorthite and bytownite compositions. The small peak at 416 cm^{-1} is due to the corundum host.

found in marble from Chillagoe, in northern Queensland, Australia (Lopez and Frost, 2015), showing major bands around 660, 610, 409, 294, and 225 cm^{-1}.

In alphabetical order, the other mineral inclusions identified were aluminite ($Al_2SO_4(OH)_4 \cdot 7H_2O$); anhydrite; apatite; barite (figure 13); chalcopyrite (figure 14); cristobalite (SiO_2); hematite; ilmenite; magnetite; near-colorless mica; monazite (figure 15); nahcolite ($NaHCO_3$); phlogopite, a pyrochlore-group mineral; spinel; and topaz. Monazite was found in one sample; the spectral match was closest to monazite-Ce, with a main band at 975 cm^{-1} and peaks at 226, 468, 623, 994, 1032, and 1060 cm^{-1} (figure 16; also compare Poitrasson et al., 2000; Nasdala et al., 2010). Topaz was only found in one sapphire (figure 17), but two isolated subhedral grains could be identified within it. Our Raman spectra were in good agreement with the reference spectra of topaz, showing main bands at 238, 265, 285, 331, 402, 455, and 925 cm^{-1} (figure 18).

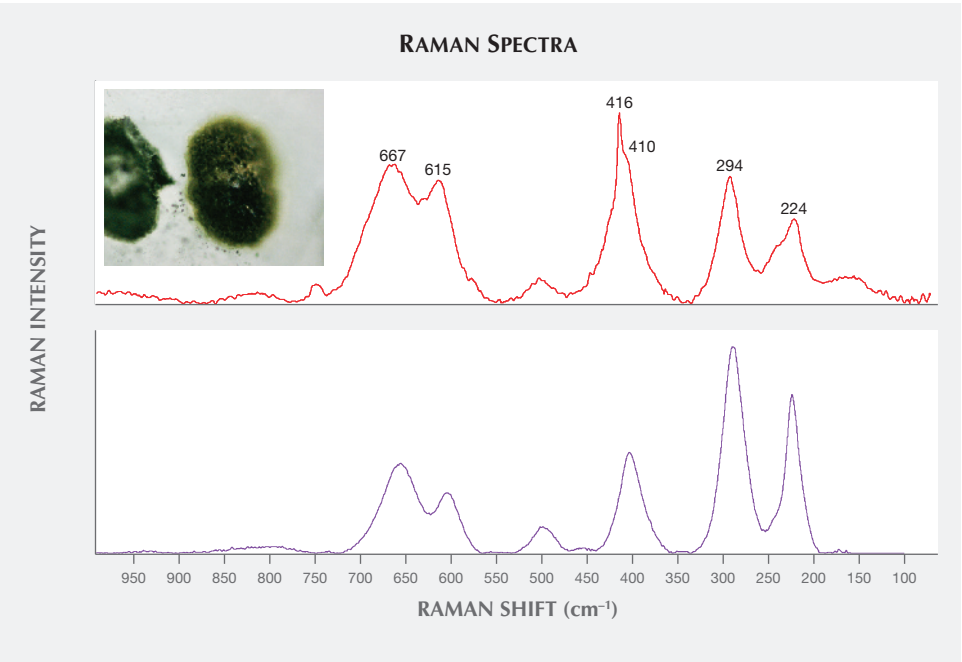

Figure 12. Allanite, a rare mineral inclusion (shown in transmitted light and oblique illumination, inset), was found in four of the sapphires examined. The Raman spectrum (top) gave a close match with allanite-Ce in the RRUFF database (bottom). The peak at 416 cm^{-1} was caused by the corundum host. Photomicrograph by Hanco Zwaan; field of view 0.7 mm.

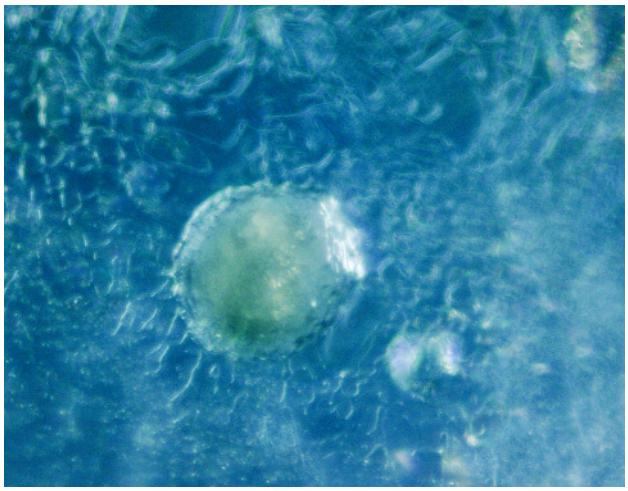

Figure 13. Barite, seen here using darkfield and oblique illumination, was found in a few samples and showed a rounded and corroded surface in all instances. Photomicrograph by Hanco Zwaan; field of view 0.35 mm.

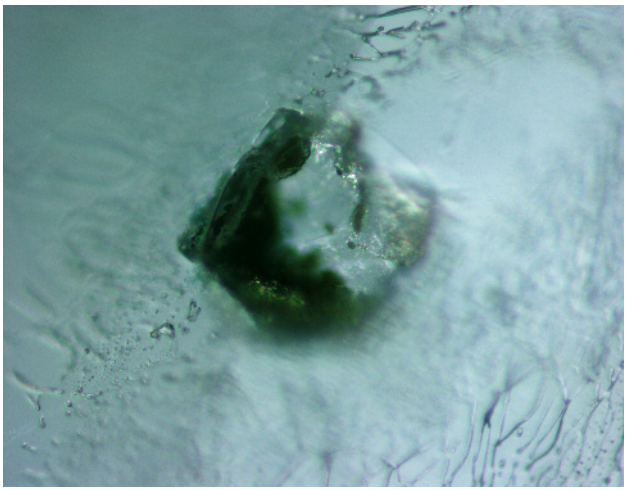

Figure 15. Monazite, shown using transmitted light and oblique illumination, has not been reported before as a mineral inclusion in alluvial Montana sapphires. Photomicrograph by Eric Buter; field of view 0.4 mm.

Raman spectra of some micas were difficult to interpret. There were spectral matches with muscovite, $KAl_2(AlSi_3O_{10})(OH,F)_2$, and often a slightly better match with the closely related (but Li-bearing) trilithionite, $K(Li,Al)_3(AlSi_3O_{10})(F,OH)_2$. For the pyrochlore-group mineral in one sapphire, a spectral match was found with "uranpyrochlore," a mineral name that has been discredited (Atencio, 2010) but essentially indicates a pyrochlore composition of $Ca_2Nb_2O_7$, possibly close to $(U,Ca,Ce)_2(Nb,Ta)_2O_6(OH,F)$. The encountered spinel-group mineral (figure 19) is difficult to characterize correctly due to existing solid solution series. When comparing spectra with principal peaks at 692 cm^{-1} (Wang et al., 2004), it can either be magnesiochromite $[Mg(Cr,Al,Fe)_2O_4]$ or an Fe-Cr spinel, with a hercynite $[FeAl_2O_4]$ and chromite $[FeCr_2O_4]$ component. The presented spectrum (figure 20) showed a principal peak with a full width at half maximum (FWHM) of about 70 cm^{-1}, which was broader than the principal peak of the matching magnesiochromite (FWHM of about 30 cm^{-1}), and another reference of chromite (FWHM of about 50 cm^{-1}; Wang et al., 2004). This could be due to heat treatment, which is known to cause lattice disorder in spinel at temperatures above 750°C, resulting in a dramatic increase of the width of the prominent feature (Saeseaw et al., 2009). The hexagonal crystal shapes appeared to be strongly determined by the host material (figure 19), indicating a syngenetic growth of spinel and corundum.

Figure 14. Chalcopyrite grains, shown here in oblique illumination, rarely occur in alluvial sapphires from Montana. Photomicrograph by Hanco Zwaan; field of view 0.7 mm.

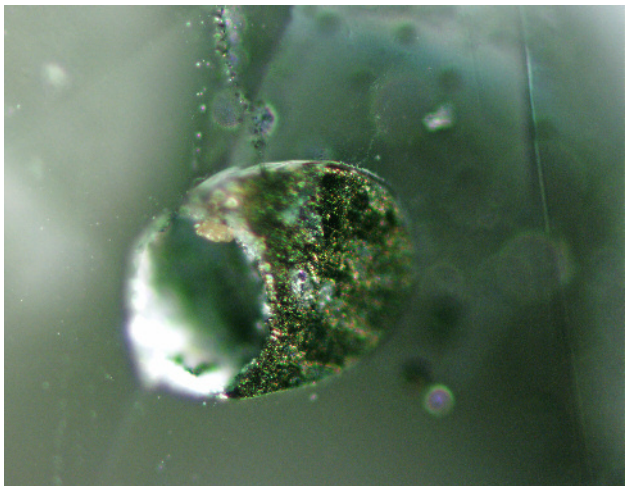

Many atoll-like inclusions, with a central mineral surrounded by a discoid stress halo, did not show clear mineral shapes but had indistinct, roundish, or elongated forms (figure 21). These inclusions did not reveal clear Raman spectra and were interpreted to be of amorphous nature, probably as a result of heat treatment.

TABLE 1. Mineral inclusions in Montana sapphires.

Minerals	Localities								
	Data from literature*								This study (mainly Rock Creek)
	Yogo Gulch	Rock Creek	Dry Cottonwood	Silver Bow	French Bar	Browns Gulch	Eldorado Bar	Montana unspecified	
Albite				Y		Y		Y	
Alkali feldspar								Y	Y
Allanite									Y
Almandine garnet	Y	Y	Y				Y		
Aluminite									Y
Analcime	Y	Y					Y	Y	
Anatase									Y
Andesine								Y	
Anhydrite			Y					Y	Y
Anorthite									Y
Apatite			Y	Y		Y		Y	Y
Baddeleyite								Y	
Barite		Y						Y	Y
Biotite	Y		Y					Y	
Boehmite							Y		
Bytownite									Y
Calcite	Y		Y				Y	Y	
Carbon (amorphous)			Y						
Carbonate		Y							
Chalcopyrite									Y
Clinozoisite		Y	Y				Y	Y	
Cristobalite									Y
Diaspore		Y	Y						
Diopside								Y	
Epidote		Y							
Ferro-columbite								Y	
Fuchsite			Y						
Gibbsite		Y							
Graphite		Y							
Hematite		Y						Y	Y
Hercynite		Y					Y	Y	
Ilmenite		Y	Y	Y		Y		Y	Y
Labradorite	Y	Y	Y						
Magnetite		Y						Y	Y
Monazite									Y
Muscovite*/Lithian mica		Y	Y					Y	Y
Nahcolite									Y
Orthoclase			Y						Y
Phlogopite	Y		Y	Y		Y	Y	Y	Y
Plagioclase							Y	Y	Y
Pyrite	Y							Y	
Pyrochlore								Y	Y
Pyroxene								Y	
Pyrrhotite			Y						
Rutile	Y	Y	Y	Y		Y	Y	Y	Y
Sphalerite			Y						
Spinel	Y			Y		Y		Y	Y
Topaz									Y
Uraninite								Y	
Zircon	Y	Y	Y		Y	Y		Y	
Zoisite		Y							

**Berg, 2007; Berg, 2014; Berger and Berg, 2006, Garland, 2002; Giuliani et al., 2007; Gübelin and Koivula, 1986; Gübelin and Koivula, 2008; Williams and Walters, 2004.*

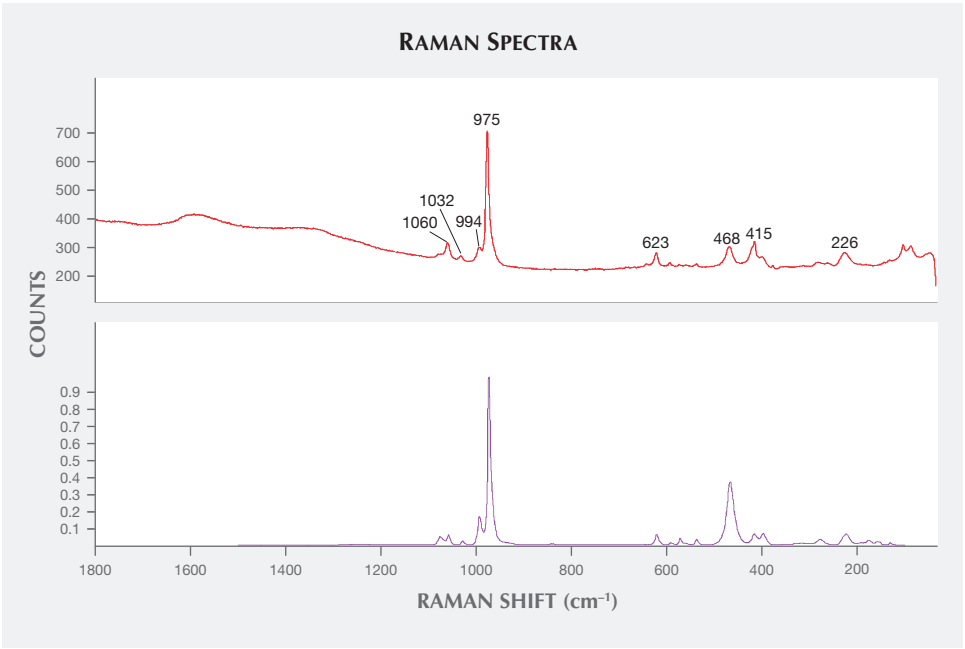

Figure 16. The Raman spectrum of the monazite inclusion (top) corresponds to a reference spectrum for monazite-Ce (bottom). The peak at 415 cm^{-1} is due to the corundum host.

The mineral inclusions found are listed along with previously published data in table 1. All of the inclusions were found in blue sapphires. Allanite, apatite, and alkali feldspar also occurred in yellow-orange and green sapphires, and Ca-rich plagioclase was encountered in green samples as well. Apart from mineral inclusions, pronounced hexagonal growth zoning (figure 10, left) and parallel growth structures (planes or lines) were encountered in many stones. These parallel growth lines may or may not be associated with color zoning (see Schmetzer and Schwarz, 2005).

Figure 17. This topaz crystal, shown using oblique illumination, was observed as a mineral inclusion in an alluvial Montana sapphire; another grain of topaz was found in the same sample. This is the first report of topaz as an inclusion in sapphire. Photomicrograph by Hanco Zwaan; field of view 1.2 mm.

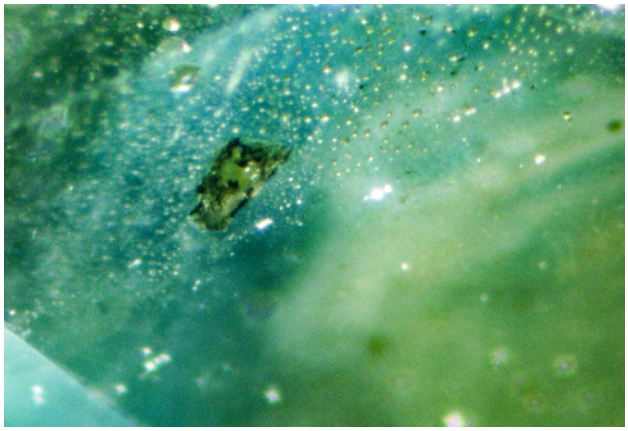

Chemical Composition. As summarized in table 2, the alluvial sapphires from Montana showed a rather consistent composition regardless of color. Whether their color was medium to dark blue, green (in some cases caused by blue and yellow zones within one stone), or orange to yellow, they had medium to high Fe (2191–7687 ppmw), low Ti and Ga (18–153 ppmw and 38–65 ppmw, respectively), and medium Mg content (35 ppmw). A green sapphire showed a low Mg content around 10 ppmw, while a dark blue sample that otherwise showed Mg values of 20 and 35 ppmw, very close to the mean value, contained one spot with a very high content of 391 ppmw. This one high value does not appear to be related to the presence of an inclusion or a different color, as values of other elements in the same spot did not reveal similar anomalies.

The higher mean Cr content in yellow to orange samples (43 ppmw) compared to blue and green (19 and 16 ppmw, respectively) is caused by one orange sapphire showing 139–155 ppmw. The other yellow and orange-yellow stones had much lower values, like most blues and greens; one dark blue sapphire also showed elevated Cr values between 91 and 100 ppmw.

Many elements had values below detection limits, with some spots giving higher values. One spot on a dark green stone showed 10 ppmw Mn. For Ni, a sin-

TABLE 2. Trace-element concentrations of Montana alluvial sapphires by LA-ICP-MS.[a]

Color	All colors		Blue		Green		Yellow-orange		
Number of samples	52		39		9		4		
Number of analyses	156		117		27		12		
Trace elements (ppmw)[b]	**Range**	**Mean**	**Range**	**Mean**	**Range**	**Mean**	**Range**	**Mean**	**Detection limits**
Li	bdl[c]–1.6		bdl		bdl–1.6		bdl		0.56–1.0
Be	bdl–0.6		bdl–0.6		bdl		bdl		0.31–1.4
B	bdl–5.4		bdl–5.4		bdl		bdl		2.2–3.4
Mg	7.1–391	35	9.4–391	37	7.1–58	29	23–49	36	0.54–1.0
Ca	bdl		bdl		bdl		bdl		107–547
Sc	bdl–1.2		bdl–1.2		bdl		bdl		0.81–1.3
Ti	18–153	58	23–142	59	18–128	50	28–153	55	0.95–4.7
V	1.1–15	5.8	1.9–15	6.1	2.1–10	5.2	1.1–6.5	3.9	0.05–0.26
Cr	bdl–155	21	bdl–100	19	2.3–48	16	4.1–155	43	1.4–4.3
Mn	bdl–10		bdl		bdl–10		bdl		0.72–1.14
Fe	2191–7687	4686	2191–7687	4598	4308–7628	5689	2259–4046	3294	4.2–6.2
Co	bdl–0.28		bdl–0.28		0.19–0.26		bdl		0.16–0.39
Ni	bdl–44		bdl–1.8		bdl–44		bdl–1.2		0.48–1.7
Zn	bdl–1.3		bdl–1.3		bdl–0.9		bdl–1.0		0.59–1.8
Ga	38–65	51	38–65	50	45–65	54	43–59	49	0.26–0.59
As	bdl–5.7		bdl–5.7		bdl–5.0		bdl–5.5		2.5–4.3
Rb	bdl–0.18		bdl–0.18		bdl		bdl		0.14–0.39
Sr	bdl–1.4		bdl–1.0		bdl–1.4		bdl–0.5		0.04–0.15
Y	bdl–0.56		bdl		bdl–0.56		bdl		0.04–0.15
Zr	bdl–0.15		bdl–0.14		bdl–0.15		bdl		0.09–0.30
Nb	bdl–0.42		bdl–0.42		bdl		bdl		0.04–0.14
Mo	bdl–2.4		bdl		bdl		bdl–2.4		0.19–0.68
Sn	bdl–13		bdl–13		bdl–11		bdl		0.10–1.3
Sb	bdl–0.73		bdl–0.49		bdl		bdl–0.73		0.29–0.78
Cs	bdl–1.1		bdl		bdl–1.1		bdl		0.07–0.80
Ba	bdl–28		bdl		bdl–28		bdl		0.19–0.59
La	bdl–6.5		bdl		bdl–6.5		bdl		0.03–0.09
Ce	bdl–15	0.12	bdl–1.6		bdl–15		bdl		0.02–0.07
Nd	bdl–4.5		bdl–0.18		bdl–4.5		bdl		0.11–0.34
Sm	bdl–0.72		bdl		bdl–0.72		bdl		0.14–0.44
Eu	bdl–0.7		bdl–0.7		bdl		bdl		0.03–0.11
W	bdl–15		bdl–15		bdl		bdl		0.06–0.19
Tl	bdl–0.68		bdl–0.68		bdl		bdl		0.03–0.10
Pb	bdl–0.19		bdl–0.07		bdl–0.19		bdl–0.18		0.03–0.15
Th	bdl–1.48		bdl		bdl–1.48		bdl		0.02–0.04

[a]*Rock Creek is the main source (see "Materials and Methods").*
[b]*The left column gives the range of concentrations for all stones; the other columns give the ranges according to color. Detection limits may vary with each analysis. Minimum detection limits are given with 99% confidence; Cu, Ge, Yb, Hf, Ta, Ir, Pt, Au, and U were below detection limits in all analyses.*
[c]*Abbreviation: bdl=below detection limit.*

gle spot on a dark green sapphire gave a value of 44 ppmw, while a few spots had values just above the detection limits. In a dark blue sample, the highest recorded value was 1.8 ppmw. Only three spots in three different stones had values ≥1 ppmw Sr. For Mo, a single spot gave 2.4 ppmw. A few measurements showed >1 ppmw Sn and Ba, while two spots were above 1 ppmw for Ce. For La and Nd, only one spot gave 6.5 ppmw and 4.5 ppmw, respectively. One analysis gave 15 ppmw W, while another indicated >1

TABLE 3. Trace-element concentrations of Montana alluvial sapphires: comparison with other data.[a]

Analytical technique	LA-ICP-MS (this study)		PIXE (Garland, 2002)					
Locality	Rock Creek[b]		Rock Creek		Dry Cottonwood Creek		Eldorado Bar	
Number of samples	52		43		15		9	
Number of analyses	156							
Trace elements (ppmw)	Range	Mean	Range	Mean	Range	Mean	Range	Mean
Ti	18–153	58	23–118	71	5–46	28	15–72	40
V	1.1–15	5.8	bdl[c]–18	7	bdl–40	6	bdl–12	5
Cr	bdl–155	21	bdl–551	65	bdl–182	26	bdl–181	44
Fe	2191–7687	4686	1120–7587	4782	1575–4596	3420	2631–6700	3866
Ga	38–65	51	42–58	49	39–77	50	46–55	51

[a]*Cu, Ge, Yb, Hf, Ta, Ir, Pt, Au, and U were below the detection limits in all analyses.*
[b]*Rock Creek is the main source (see "Materials and Methods").*
[c]*Abbreviation: bdl=below detection limit.*

ppmw Th. All other elements analyzed showed values below or only slightly above detection limits (table 2).

Proton-induced X-ray emission (PIXE) analyses of a similar number of samples (Garland, 2002) for Ti, V, Cr, Fe, and Ga (table 3), showed comparable ranges and mean values. The only exception was Cr, for which PIXE analysis showed a wider range of values in the Rock Creek samples. This is because the suite of 43 sapphires analyzed by Garland (2002) contained six pink samples along with the blue, green, and yellow varieties.

DISCUSSION

Mineral Inclusions. The inclusions are listed in table 1 and compared with previously published data by Gübelin and Koivula (1986, 2008), Garland (2002), Williams and Walters (2004), Berger and Berg (2006), Berg (2007, 2014), and Giuliani et al. (2007). Our study showed the presence of allanite, anatase, chalcopyrite, monazite, and topaz, which were previously unreported, although Berg (2014) inferred the presence of allanite in one sapphire using EDX analysis. Orthoclase and Ca-rich plagioclase (anorthite-

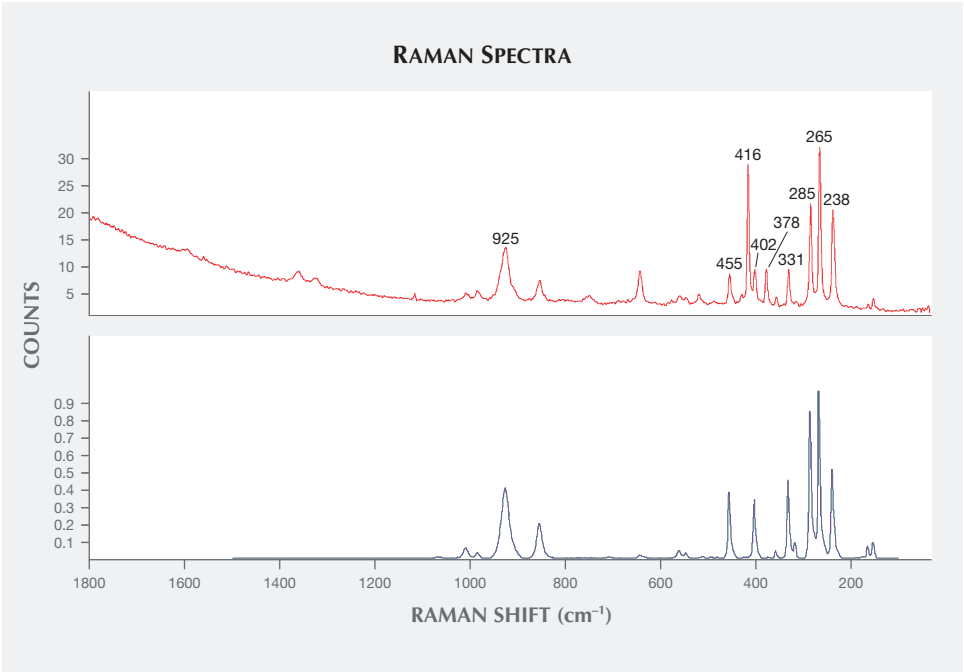

Figure 18. The Raman spectrum of the topaz inclusions (top) compared well with the reference spectrum (bottom). The peaks at 416 and 378 cm^{-1} are due to the sapphire host.

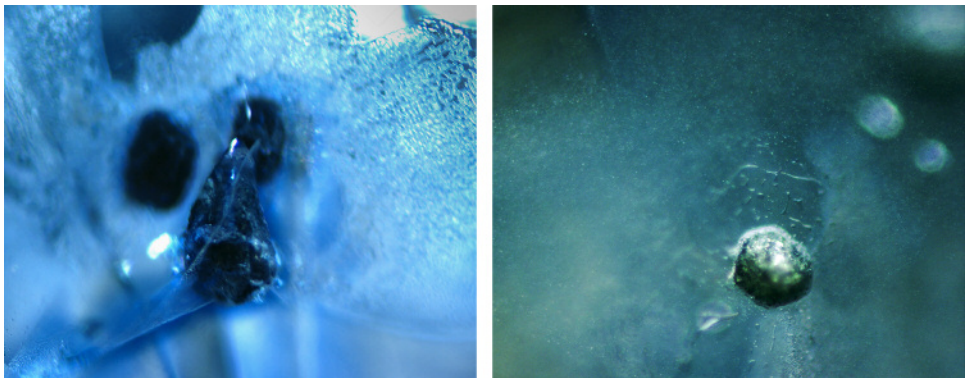

Figure 19. Spinel inclusions showed a hexagonal outline, indicating syngenetic growth. Rutile inclusions appear in the background of the photomicrograph on the left. The images are shown in transmitted light (left) and oblique illumination (right). Photomicrographs by Hanco Zwaan; field of view 1.4 mm (left) and 0.7 mm (right).

bytownite) were similar to earlier reported alkali feldspar and labradorite, respectively, whereas phlogopite was consistent with the earlier mention of biotite. In the gemological literature, allanite has been described as an inclusion indicative of a Kashmir origin (Schwieger, 1990), but obviously can no longer be considered a hallmark for that locality. Moreover, allanite has also been found in corundum from Rio Mayo, Colombia (Sutherland et al., 2008).

The predominance of rutile—in many cases the only mineral present—appears to confirm Rock Creek as the most likely sample location, as opposed to Dry Cottonwood Creek and Eldorado Bar (compare with, e.g., Guo et al., 1996; Gübelin and Koivula, 2008; Berg, 2007, 2014). Hexagonal zoning, enhanced by exsolved rutile needles, is regarded as the most evident inclusion feature in alluvial Montana sapphires (Gübelin and Koivula, 2008). The frequent absence of these inclusions, combined with the presence of blue halos around small rutile crystals, confirmed that the samples were heat-treated (compare with Emmett and Douthit, 1993; Gübelin and Koivula, 2008). The strong blue halos are caused by internal diffusion of titanium from rutile into the iron-bearing corundum host during high-temperature treatment (Koivula, 1987). In addition to the blue halos, the most common internal features in heat-treated blue to blue-green alluvial Montana sapphires are blue irregular spots, single blue straight lines, multiple parallel straight lines, and blue hexagonal patterns of parallel straight lines (Kane, 2008). Heat treatment might also be the reason why barite grains

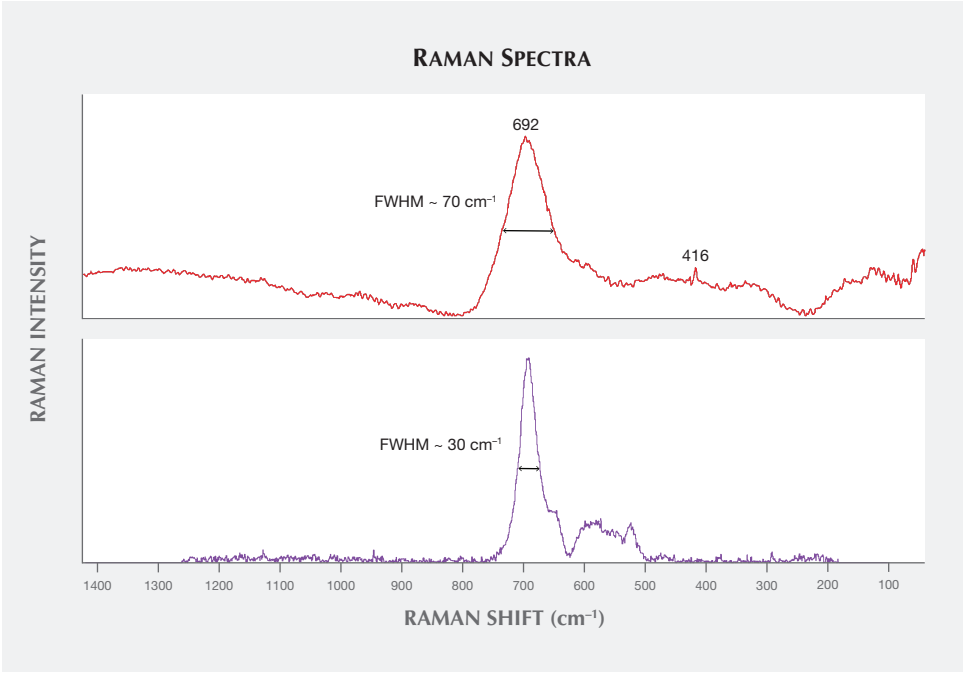

Figure 20. The Raman spectrum of a spinel-group inclusion (top) showed a principal band at 692 cm^{-1} with a FWHM around 70 cm^{-1}. This is broader than the reference spectrum of magnesiochromite and published chromite spectra (bottom), which could be due to heat treatment. The small peak at 416 cm^{-1} was caused by the sapphire host.

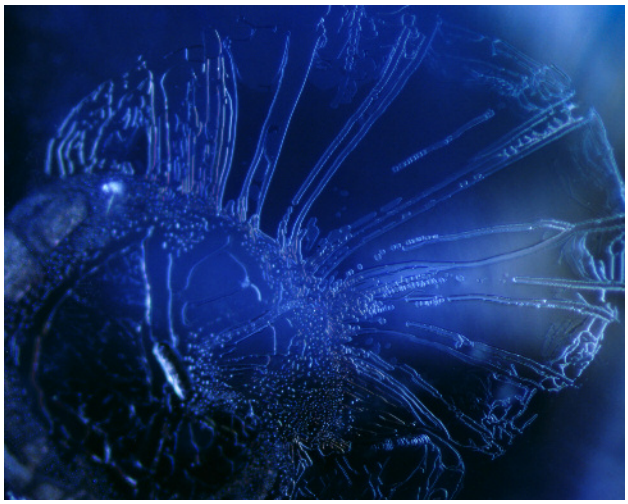

Figure 21. Atoll-like inclusions were common, with a central mineral surrounded by roundish or elongated shapes. The inclusions are seen here with darkfield and oblique illumination. Photomicrograph by Hanco Zwaan; field of view 1.4 mm.

showed a rounded and corroded or partially molten surface (figure 13), as blue and green sapphires are heated at 1650°C (Emmett and Douthit, 1993) and the melting point of barite is 1580°C.

The heat treatment routine demands further caution when interpreting the results. Aluminite, a clay-like hydrated/hydrous aluminum sulfate, and nahcolite ($NaHCO_3$), which occurred as a captured phase in a fluid inclusion, were both found in partially healed, surface-reaching fissures. In those fissures, several expanded "snowball"-like inclusions were also present, and therefore both minerals are interpreted as phases related to heat treatment, probably formed during post-treatment cooling. Nahcolite has been found in fluid inclusions in magmatic, metamorphic, and metasomatic rocks (e.g., pegmatites, carbonatites, basaltic glasses, eclogites, granulites, and alkaline metasomatic alteration zones), but is only stable at relatively low temperatures (<600°C, virtually pressure-independent). In natural occurrences, nahcolite is likely a daughter mineral that crystallized from the included fluids as temperature decreased (Liu and Fleet, 2009). As nahcolite was only encountered incidentally, and appears to be related to features caused by heating, it is highly unlikely to be a daughter mineral of natural origin in the sapphires we analyzed.

The low-pressure silica polymorph cristobalite, which is stable above 1470°C at 1 bar pressure but can persist metastably to much lower temperatures (e.g., Deer et al., 2004), was detected in relation to the atoll-like inclusions as ovoid or snowball-like features. Cristobalite is therefore regarded as another result of heat treatment, due to either crystallization out of a molten flux when cooling is not too rapid (compare with Emmett et al., 2003) or the heating of natural glass inclusions. Those inclusions were reported in unheated Rock Creek sapphires by Gübelin and Koivula (2008).

The interior surfaces of negative crystals strongly resembled the dendritic patterns of resolidified surfaces, seen in many high-temperature heat-treated sapphires (Gübelin and Koivula, 2008), and are therefore interpreted as a result of heat treatment as well.

Mineral Inclusions and Provenance. Topaz, barite, apatite, monazite, pyrochlore, anatase, allanite, and K-feldspar inclusions in corundum suggest the involvement of pegmatites and related veins during formation, and/or an environment rich in *incompatible elements* and volatiles such as in alkali magmas (Giuliani et al., 2007) and carbonatites (Guo et al., 1996). The presence of chromite-spinel and Ca-rich plagioclase, however, would indicate an ultramafic to mafic igneous source. As a result of metasomatism, phlogopite is often present in association with ultramafic intrusions. Metasomatism is critical to the genesis of many gem corundum deposits, and desilication of an intrusive pegmatite in ultramafic/mafic rock by contact metasomatism is described as a corundum-forming process (e.g., Giuliani et al., 2007; Simonet et al., 2008). Rutile occurred in many of the sapphires from the present study, but particularly in two stones that also contained either chromite-spinel or plagioclase. Yet rutile cannot be considered a possible indicator of source, as it is known to occur in corundum from various origins (e.g., Gübelin and Koivula, 1986, 2008; Smith, 2010).

Mineral inclusions that might be indicative of particular growth environments were found in different samples. This leaves open the possibility that the alluvial sapphires have different sources, as proposed by Berger and Berg (2006). Chemical analyses of the alluvial Montana sapphires containing the particular inclusions mentioned above were further evaluated for any supporting evidence.

Chemical Composition. Various geochemical plots of trace-element concentrations and ratios have been used to distinguish between sapphires of various localities and of different origins (e.g., Sutherland et al.,

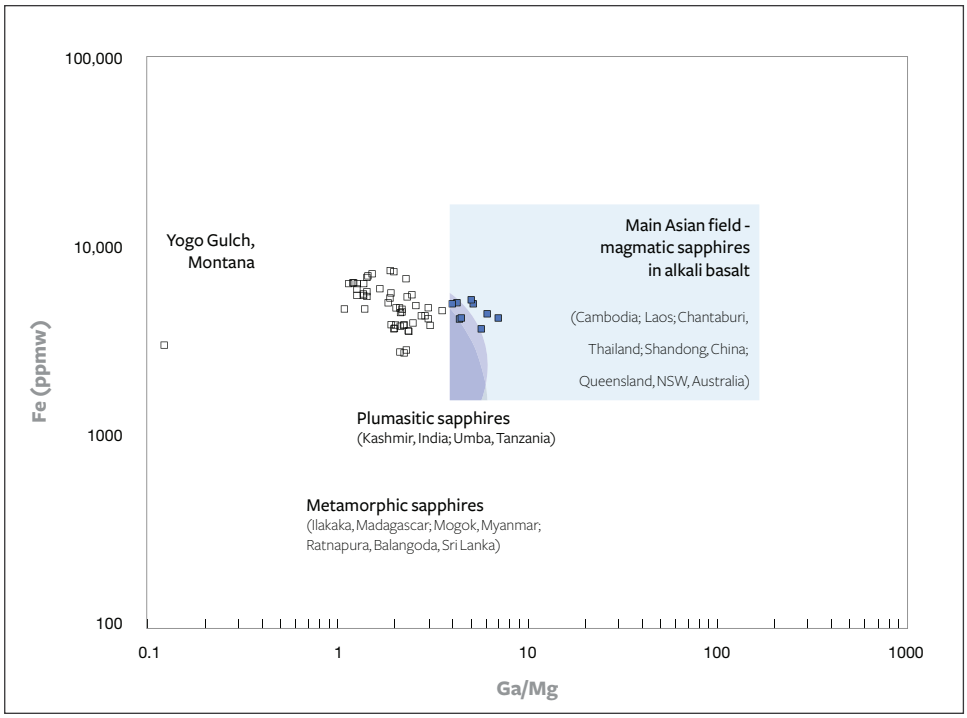

Figure 22. Compositions of alluvial Montana sapphires (blue, green and red squares) in relation to metamorphic, magmatic and blue plumasitic sapphires (shaded compositional ranges), as shown by Peucat et al. (2007). Red symbols indicate sapphires that contained inclusions suggesting a volatile-rich formation environment, and green symbols represent sapphires that contained inclusions of possible ultramafic/mafic origin. The blue symbols refer to the compositions of the other sapphires analyzed. For further explanation, see text.

1998; Zaw et al., 2006; Peucat et al., 2007; Sutherland and Abduriyim, 2009). The use of the Ga/Mg ratio versus Fe concentration appears to be an efficient tool to discriminate between the "metamorphic" sapphires, found mainly in metamorphic terrains, and the "magmatic" samples found mainly in alkali basalts and syenite (Peucat et al., 2007; Sutherland and Abduriyim, 2009). Metasomatic (specifically "plumasitic") sapphires can also be plotted in this diagram. These specimens, found in primary metasomatic rocks, are related to fluid interactions between ultramafic/mafic rocks such as serpentinites, amphibolites, and marbles, and aluminum-rich rocks, including granites, pegmatites, and paragneisses such as metapelites (Lawson, 1903; Du Toit, 1946; Peucat et al., 2007). Plumasites are corundum-bearing metasomatic rocks that result from the desilication of ultramafic-intruding pegmatites. Sapphire deposits in both Kashmir (India) and Umba (Tanzania) are closely related to plumasites (Simonet et al., 2008).

The alluvial Montana sapphires largely plotted in a restricted area (figure 22) and did not provide supporting evidence for different sources. The samples that contained inclusions indicative of different growth environments showed completely overlapping compositions. Even in one sapphire containing topaz inclusions (M037), the measured Ga/Mg ratio varied between 1.0 and 2.8 (with Fe between 5315 and 4795 ppmw, respectively), which comprised the Ga/Mg ratio of the bulk of the samples. Also, there were no discernible trends pertaining to Cr, Ti, V, and Ca.

Figure 23. Compositions of alluvial Montana samples in an Fe-Mg-Ti (ppmw) diagram, showing overlap with metamorphic sapphires from Mogok, Myanmar; metasomatic sapphires from Umba, Tanzania; and sapphires from Rio Mayo, Colombia. Based on this diagram, metasomatic sapphires from Kashmir can be unambiguously separated from alluvial Montana samples.

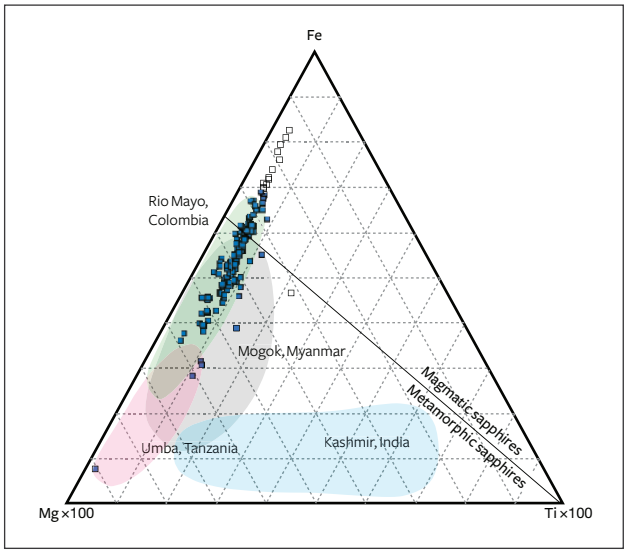

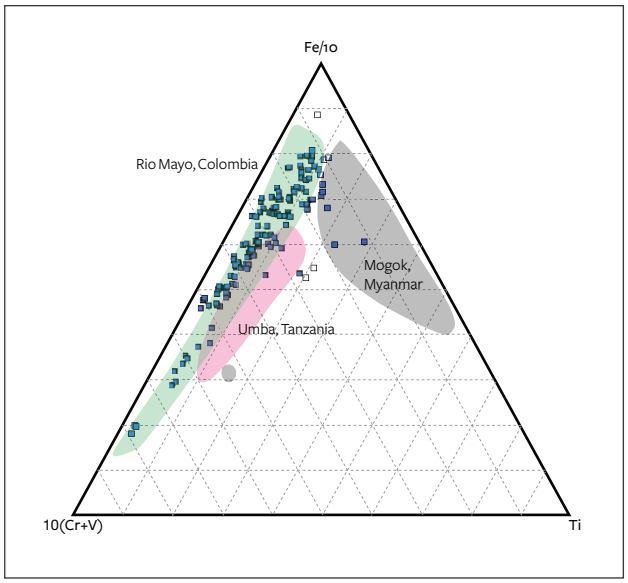

Figure 24. Alluvial Montana sapphires follow the same trend as those from Rio Mayo, Colombia, and Umba, Tanzania, but can be separated from Mogok sapphires, although individual analyses may show overlap, based on this Fe-(Cr+V)-Ti diagram.

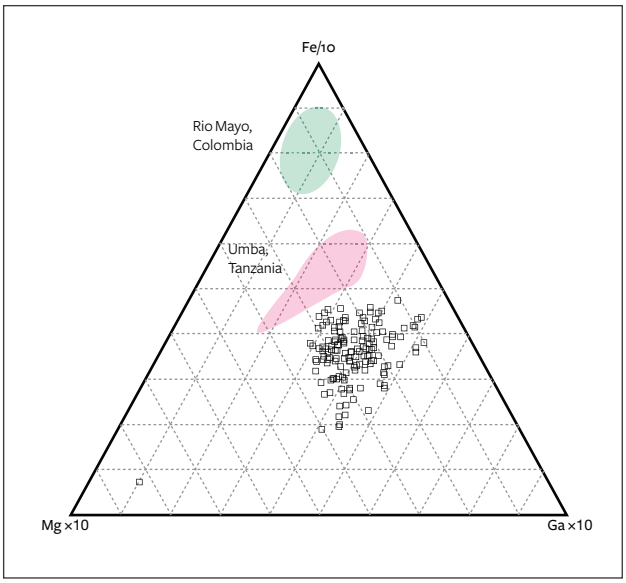

Figure 25. This Fe-Mg-Ga diagram shows a clear compositional difference between alluvial Montana sapphires and sapphires from Umba and from Rio Mayo.

Comparing chemical compositions with the large dataset of many sapphire occurrences published by Peucat et al. (2007), and with data for Australian samples (Sutherland and Abduriyim, 2009), the alluvial Montana sapphires can be separated clearly from primary sapphires found at Yogo Gulch, Montana, which are thought to be of mantle origin (see the introduction). Alluvial Montana sapphires plotted in the fields of metamorphic and plumasitic/metasomatic sapphires, with a slight overlap into the magmatic sapphires field (figure 22). Within the metamorphic sapphires, the most overlap occurred with those from Mogok, Myanmar (formerly Burma), which showed a relatively high Fe content (1200–4800 ppmw). The Montana sapphires' composition further overlapped with alluvial samples from Rio Mayo, Colombia. The Colombian sapphires were considered difficult to pinpoint (Peucat et al., 2007). They showed a heterogeneous Fe composition (light blue 2500–4000 ppmw, and dark blue approximately 14,000 ppmw) and a relatively low Ga/Mg ratio (an average ratio of 1.12), indicating that they are different from magmatic types of alkali basalts and geochemically more allied to metamorphic blue sapphires. Sutherland et al. (2008) concluded that Colombian sapphires geochemically fall within the limits of metasomatic, desilicated felsic/ultramafic "plumasitic" associations, supported by high U/Th ratios in included zircon, reflecting a direct metasomatic fluid-rich input for the corundum genesis.

Plotted on an Fe-Mg-Ti diagram, the Montana alluvial sapphires follow the same trend as sapphires from Umba and Rio Mayo and, like the Colombian sapphires, cross the magmatic and metamorphic fields (figure 23). In this diagram, the Montana samples also show an overlap with Mogok material but do not follow the Ti-rich trend of Kashmir sapphires. Although the Montana sapphires cross the magmatic field, they do not follow the clear Fe-Ti trend of most magmatic sapphires (compare Peucat et al., 2007).

The overlapping occurrences can be further separated using a ternary Fe-(Cr+V)-Ti diagram (figure 24). Again, the Montana sapphires follow the same trend as Colombian and Tanzanian sapphires but can largely be distinguished from Burmese sapphires. Plotting slightly toward Ga, they can also be separated from the sapphires of Umba and Rio Mayo in an Fe-Mg-Ga diagram (figure 25).

Other combinations and plots that appeared to be effective in characterizing corundum from Australia, such as Fe/Ti vs. Cr/Ga and Ga/Mg vs. Fe/Mg (Sutherland and Abduriyim, 2009; Sutherland et al., 2009), gave mixed results for alluvial Montana sapphires. They plotted in between metamorphic and magmatic fields, or in both fields, although in the latter combination most of the analyses plotted in the metamorphic field.

Another factor that clearly separates alluvial

Montana sapphires from both magmatic blue sapphires from alkali basalts and syenitic blue sapphires is their 10,000 × Ga/Al ratios, between 0.7 and 1.2. This range is in agreement with values of the continental crust (1.0–1.5) and much lower than that of magmatic sapphires, which vary between 2.5 and 3.7 (Peucat et al., 2007).

Regression is a technique for determining the statistical relationship between two or more variables where a change in a dependent variable is associated with, and depends on, a change in one or more independent variables. Discriminant analysis is a regression-based statistical technique that can be used to determine the classification or group of a particular stone on the basis of its characteristics or essential features. It differs from techniques such as cluster analysis (the demonstrated chemical plots are examples of cluster analysis) in that the classifications or groups to choose from must be known in advance. Each case must have a score on one or more quantitative predictor measures as well as a score on a group measure.

Statistical determination of the most probable deposit type for secondary placer corundum deposits is based on the calculation of discriminating factors from the concentration of oxides in corundum from the main primary deposits (Giuliani et al., 2014). As explained above, the discriminating factors are determined by a statistical analysis that tries to minimize the variance in a certain class (e.g., sapphires of plumasitic origin) while maximizing the variance between classes (e.g., between sapphires of plumasitic and syenitic origin).*

Discriminant analysis of sapphire and ruby deposits in Madagascar has shown its effectiveness in determining the most likely deposit type, although Giuliani et al. (2014) demonstrated that this method needs improvement. For example, for sapphires of plumasitic origin, the discriminant analysis showed two subclasses (P1 and P2), of which P1 shows slight overlap with samples of syenitic origin. Further systematic geological study of the plumasitic primary sapphire occurrences should lead to a more refined typology. Interestingly, when recalculating our analyses of Fe, Cr, V, Ti, Mg, and Ga from ppmw to oxides in weight percent and applying this technique, the alluvial Montana sapphires plot largely in or very close to the field of primary sapphires of plumasitic origin (subclass P1, figure 26). This independent statistical method appears to support a close geochemical affinity between alluvial Montana sapphires and sapphires of plumasitic/metasomatic origin.

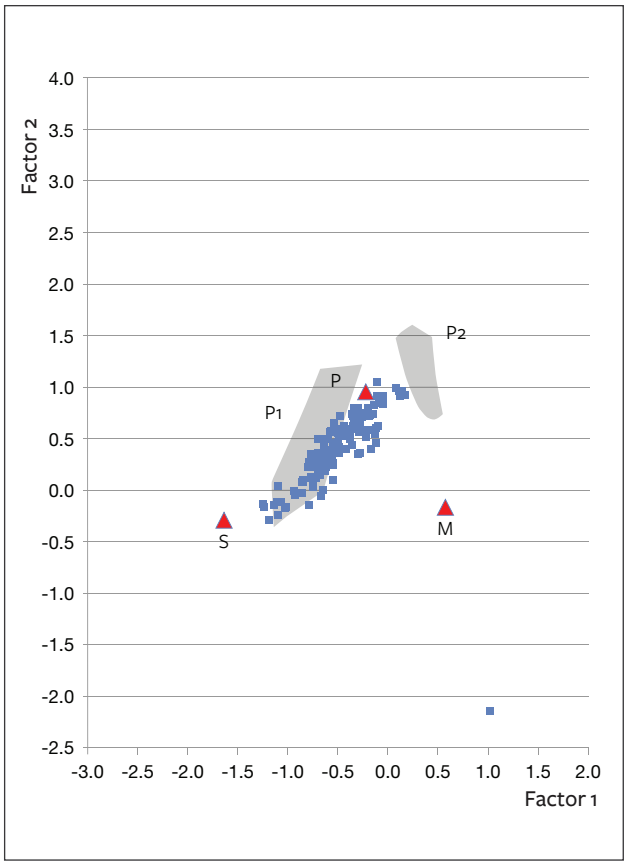

Figure 26. Discriminant analysis of alluvial Montana samples shows that they plot approximately in the field of primary sapphires of plumasitic origin. P1 and P2 are two subclasses of primary sapphires of plumasitic origin. The red triangles represent the centroids of spaces related to sapphires of syenitic origin (S), plumasitic origin (P), and metasomatic/metamorphic origin (M; compare with Giuliani et al., 2014).

*The two discriminant factors are defined as:

Factor 1 = 0.23095 × (Cr_2O_3 – 0.0613814)/0.0596296 – 0.723839 × (FeO – 0.489593)/0.372367 – 0.0403934 × (Ga_2O_3 – 0.0159195)/0.00946033 + 0.0767757 × (MgO – 0.00613983)/0.0040002 – 0.00901195 × (TiO_2 – 0.0236271)/0.0567399 + 0.0791335 × (V_2O_3 – 0.00402119)/0.00329669

Factor 2 = –0.530426 × (Cr_2O_3 – 0.0613814)/0.0596296 – 0.638704 × (FeO – 0.489593)/0.372367 – 0.00893226 × (Ga_2O_3 – 0.0159195)/0.00946033 – 0.200622 × (MgO – 0.00613983)/0.0040002 + 0.296868 × (TiO_2 – 0.0236271)/0.0567399 – 0.165072 × (V_2O_3 – 0.00402119)/0.00329669

Figure 27. The features of Montana alluvial sapphires indicate a metasomatic origin. They can be separated from material with overlapping properties through their distinct chemical composition. Photo by Robert Weldon/GIA.

Implications for the Original Source of Corundum. Geochemically, the samples in this study were most similar to plumasitic/metasomatic sapphires, as well as metamorphic sapphires from Mogok. The plumasitic sapphires from Kashmir and Umba are related to metasomatic alterations where pegmatites depleted in SiO_2 and ultramafic rocks are in contact (e.g., Solesbury, 1967; Atkinson and Kothavala, 1983; Seifert and Hyršl, 1999; Giuliani et al., 2007; Peucat et al., 2007). In the Mogok material, metasomatic exchanges are likely in a complex setting where sapphires are present in "urtite" dikes (rocks containing more than 70% nepheline) and have developed in marble during high-grade metamorphism, with probable interactions with nearby granites (Iyer, 1953; Kane and Kammerling, 1992; Harlow, 2000; Peucat et al., 2007).

The Montana sapphires, showing a similar homogeneous chemical composition, have inclusions that suggest an environment containing *volatile components* (F, OH, P) and incompatible elements (Ba, Ce, Nd, Nb, and possibly Y, La, Ta, Nd, and Th) but that also hint at the presence of ultramafic/mafic rocks. It is therefore also plausible that the alluvial sapphires from Montana were formed during metasomatic alterations between Al- and Mg-rich units.

Involvement of F-rich fluids is supported by the presence of topaz, apatite, and pyrochlore inclusions, and also by the low Ga/Al ratios in the sapphires, which may be caused by extraction of GaF_6^{3-} ions during F-rich fluid circulation. Whalen et al. (1987) explained that this process occurred during partial melting in granulites in the presence of F-rich fluids, depleting granulite restites and enriching the melt in Ga.

Garland (2002) advocated a metamorphic *sensu stricto* origin in a closed system of Montana sapphires (see "Geology and Origin" above), but at the same time recognized that the assumption of equilibrium in the corundum-anorthite-clinozoisite-muscovite assemblage is a problem. No reaction between

corundum and clinozoisite became evident, and there is no indication of an equilibrium relationship between the host and inclusions. Moreover, neither clinozoisite nor zoisite inclusions were found in our study.

Garland (2002) also stated that the Montana sapphires may have formed in the metamorphic events related to the intrusion of the Idaho batholith into largely aluminous Proterozoic metamorphic rocks at the northern and western edge of the batholith (again, see figure 3). The main intrusive phases are late Cretaceous, with smaller associated Tertiary plutons, which developed large hydrothermal systems with associated metasomatism. This would suggest the presence of a more open system during the formation of Montana sapphires, in line with our data and observations.

CONCLUSIONS

Geochemical features of alluvial sapphires from Montana (figure 27) show significant overlap with trends of plumasitic/metasomatic sapphires. These features and the mineral inclusions identified may reflect a metasomatic origin. Topaz inclusions were observed in one of the samples. Topaz has not been reported as an inclusion in sapphire from any other occurrence, and it may serve to prove a Montana origin. The alluvial Montana sapphires can further be geochemically characterized and distinguished from occurrences with the most overlapping properties (Umba, Tanzania, and Rio Mayo, Colombia) by using concentrations and ratios of Fe, Ga, Mg, Ti, Cr, and V and a combination of Fe-Ga/Mg, Fe-Mg-Ti, Fe-(Cr+V)-Ti, and Fe-Mg-Ga diagrams.

GLOSSARY

Batholith: a large, igneous rock or intrusive body formed at great depth, having an aerial extent of at least 100 km^2 (40 sq. mi) and no known floor.

Foreland basin: a linear sedimentary basin at a foreland, the exterior area of an orogenic belt where deformation occurs without significant metamorphism. Generally the foreland is the portion of the orogenic belt closest to the continental interior.

Hydrothermal breccia: a rock composed of angular broken rock fragments held together by a mineral cement or in a fine-grained matrix. It is formed when hydrothermal fluid fractures a rock mass.

Incompatible element: 1. An element for which the ratio of mineral or mineral assemblage to liquid is much less than unity; in other words, the element is concentrated in the liquid. 2. A chemical element that tends to remain in the melt when a magma crystallizes.

Nonconformity: a substantial break or gap in the geologic record where a rock is overlain by another that is not next in stratigraphic succession, such as an interruption in the continuity of a depositional sequence of sedimentary rocks or a break between eroded igneous rocks and younger sedimentary strata. It normally implies uplift and erosion with loss of the previously formed record.

Volatile component: a material in a magma, such as water or carbon dioxide, whose vapor pressure is sufficiently high to be concentrated in a gaseous phase.

Main source: Jackson (1997)

ABOUT THE AUTHORS

Dr. Zwaan is head of the Netherlands Gemmological Laboratory and researcher at Naturalis Biodiversity Center in Leiden, the Netherlands. Mr. Buter is associate researcher, also at Naturalis. Dr. Mertz-Kraus is a scientific staff member of the Petrology Group at the Institut für Geowissenschaften, Johannes Gutenberg-Universität, in Mainz, Germany. Mr. Kane is president and CEO of Fine Gems International, in Helena, Montana.

ACKNOWLEDGMENTS

The anonymous peer reviewers are thanked for their valuable comments and suggestions. Dirk van der Marel is thanked for assistance with photography and preparing graphics.

REFERENCES

Atencio D., Andrade M.B., Christy A.G., Gieré R., Kartashov P.M. (2010) The pyrochlore supergroup of minerals: nomenclature. *Canadian Mineralogist*, Vol. 48, No. 3, pp. 673–698, http://dx.doi.org/10.3749/canmin.48.3.673

Atkinson D., Kothavala R. (1983) Kashmir sapphire. *G&G*, Vol. 19, No. 2, pp. 64–76, http://dx.doi.org/10.5741/GEMS.19.2.64

Baker D.W. (1992) Central Montana alkali province: critical review of Laramide plate tectonic models that extract alkali magmas from abnormally thick Precambrian lithospheric mantle. *Northwest Geology*, Vol. 20/21, pp. 71–95.

——— (1994) Montana sapphires – the value of color. *Northwest Geology*, Vol. 23, pp. 61–75.

Berg R.B. (2007) *Sapphires in the Butte-Deer Lodge Area, Montana*. Montana Bureau of Mines and Geology, Bulletin 134, 59 pp.

——— (2011) Bedrock source of sapphires in alluvial deposits in the Rock Creek, sapphire district, Western Montana. *Geological Society of America, Abstracts with Programs*, Vol. 34, No. 4, p. 9.

——— (2014) *Sapphires in the Southwestern Part of the Rock Creek Sapphire District, Granite County, Montana*. Montana Bureau of Mines and Geology, Bulletin 135, 85 pp.

Berger A.L., Berg R.B. (2006) The Silver Bow sapphire occurrence, Montana: Evidence for a volcanic bedrock source for Montana's alluvial sapphire deposits. *Economic Geology*, Vol. 101, No. 3, pp. 679–684, http://dx.doi.org/10.2113/gsecongeo.101.3.679

Cade A., Groat L.A. (2006) Garnet inclusions in Yogo sapphires. *G&G*, Vol. 42, No. 3, p. 106.

Clabaugh S.E. (1952) *Corundum Deposits in Montana*. U.S. Geological Survey, Bulletin 983, 100 pp.

Deer W.A., Howie R.A., Wise W.S., Zussman J. (2004) *Rock-Forming minerals: Framework Silicates. Silica Minerals, Feldspathoids and the Zeolites*. The Geological Society, London, Volume 4B, 2nd ed., 982 pp.

Du Toit A.L. (1946) Discussion on 'corundum indicator basic rocks and associated pegmatites in the Northern Transvaal by J.W. Brandt'. *Transactions of the Geological Society of South Africa*, Vol. 49, pp. 51–102.

Emmett J.L., Douthit T.R (1993) Heat treating the sapphires of Rock Creek, Montana. *G&G*, Vol. 29, No. 4, 250–272, http://dx.doi.org/10.5741/GEMS.29.4.250

Emmett J.L., Scarratt K., McClure S.F., Moses T., Douthit T.R., Hughes R., Novak S., Shigley J.E., Wang W., Bordelon O., Kane R.E. (2003) Beryllium diffusion of ruby and sapphire. *G&G*, Vol. 39, No. 2, pp. 84–135, http://dx.doi.org/10.5741/GEMS.39.2.84

Evans K.V., Aleinikoff J.N., Obradovich J.D., Fanning M. (2000) SHRIMP U-Pb geochronology of volcanic rocks, Belt Supergroup, western Montana: evidence for rapid deposition of sedimentary strata. *Canadian Journal of Earth Sciences*, Vol. 37, No. 9, pp. 1287–1300, http://dx.doi.org/10.1139/e00-036

Freeman J.J., Wang A., Kuebler K.E., Jolliff B.L., Haskin L.A. (2008) Characterization of natural feldspars by Raman spectroscopy for future planetary exploration. *The Canadian Mineralogist*, Vol. 46, No. 6, pp. 1477–1500.

Fuentes F., DeCelles P.G., Constenius K.N. (2012) Regional structure and kinematic history of the Cordilleran fold-thrust belt in northwestern Montana, USA. *Geosphere*, Vol. 8, No. 5, pp. 1104–1128, http://dx.doi.org/10.1130/GES00773.1

Garland M.A. (2002) The Alluvial Sapphire Deposits of Western Montana. PhD thesis, University of Toronto, Canada, 343 pp.

Giuliani G., Ohnenstetter D., Garnier V., Fallick A.E., Rakotondrazafy M., Schwarz D. (2007) The Geology and Genesis of Gem Corundum Deposits. *Mineralogical Association of Canada, Short Course Series* Vol. 37, pp. 23–78.

Giuliani G., Caumon G., Rakotosamizanany S., Ohnenstetter D., Rakotondrazafy M. (2014) Classification chimique des corindons par analyse factorielle discriminante: application a la typologie des gisements de rubis et saphirs. *Revue de l'Association Française de Gemmologie*, No. 188, pp. 14–22.

Gübelin E.J., Koivula J.I. (1986) *Photoatlas of Inclusions in Gemstones*. ABC Edition, Zurich, Switzerland.

——— (2008) *Photoatlas of Inclusions in Gemstones*, Vol. 3. Opinio Publishers, Basel, Switzerland.

Guo J., O'Reilly S.Y., Griffin W.L. (1996) Corundum from basaltic terrains: a mineral inclusion approach to the enigma. *Contributions to Mineralogy and Petrology*, Vol. 122, No. 4, pp. 368–386, http://dx.doi.org/10.1007/s004100050134

Harlow G.E. (2000) The Mogok Stone Tract, Myanmar: minerals with complex parageneses. *Minerals and Museums 4 Conference Abstracts*, Melbourne, Australia, http://research.amnh.org/users/gharlow/MogokAbsDistrib.pdf

Iyer L.A.N. (1953) The geology and gemstones of the Mogok Stone Tract, Burma. *Memoirs of the Geological Survey of India*, Vol. 82, p. 100.

Jackson J.A. (1997) *Glossary of Geology*, 4th ed. American Geological Institute, Alexandria, VA, 769 pp.

Jochum K.P., Nohl U., Herwig K., Lammel E., Stoll B., Hofmann A.W. (2005) GeoReM: a new geochemical database for reference materials and isotopic standards. *Geostandards and Geoanalytical Research*, Vol. 29, No. 3, pp. 333–338, http://dx.doi.org/10.1111/j.1751-908X.2005.tb00904.x

Jochum K.P., Weis U., Stoll B., Kuzmin D., Yang Q., Raczek I., Jacob D.E., Stracke A., Birbaum K., Frick D.A., Günther D., Enzweiler J. (2011) Determination of reference values for NIST SRM 610-617 glasses following ISO guidelines. *Geostandards and Geoanalytical Research*, Vol. 35, No. 4, pp. 397–429, http://dx.doi.org/10.1111/j.1751-908X.2011.00120.x

Kane R.E. (2004) The sapphires of Montana: A rainbow of color. *Gem Market News*, Vol. 22, No. 1, Pt. 1, pp. 1–8.

——— (2008) American sapphires: Montana and Yogo. *World of Gems Conference 2008*, Gemworld International, Glenview, IL, pp. 59–64.

Kane R.E., Kammerling R.C. (1992) Status of ruby and sapphire mining in the Mogok Stone Tract. *G&G*, Vol. 28, No. 3, pp. 152–174, http://dx.doi.org/10.5741/GEMS.28.3.152

Koivula J.I. (1987) Internal diffusion. *Journal of Gemmology*, Vol. 20, Nos. 7/8, pp. 474–477.

Lawson A.C. (1903) Plumasite, an oligoclase corundum rock, near Spanish Peak, California. *University of California Publications in Geological Sciences*, pp. 219–229.

Liu X., Fleet M.E. (2009) Phase relations of nahcolite and trona at high *P-T* conditions. *Journal of Mineralogical and Petrological Sciences*, Vol. 104, No. 1, pp. 25–36, http://dx.doi.org/10.2465/jmps.080402

López A., Frost R.L. (2015) Identification of allanite (Ce, Ca, Y)$_2$(Al, Fe^{3+})$_3$(SiO_4)$_3$OH found in marble from Chillagoe, Queensland using Raman spectroscopy. *Spectrochimica Acta Part A: Molecular and Biomolecular Spectroscopy*. Vol. 138, pp. 229–233, http://dx.doi.org/10.1016/j.saa.2014.11.052

May T.W., Wiedmeyer R.H. (1998) A table of polyatomic interferences in ICP-MS. *Atomic Spectroscopy*, Vol. 19, No. 5, pp. 150–155.

Mychaluk K.A. (1995) The Yogo sapphire deposit. *G&G*, Vol. 31, No. 1, pp. 28–41, http://dx.doi.org/10.5741/GEMS.31.1.28

Nasdala L., Grötzschel R., Probst S., Bleisteiner B. (2010) Irradiation damage in Monazite-(Ce): an example to the limits of Raman confocality and depth resolution. *Canadian Mineralogist*, Vol. 48, pp. 351–359, http://dx.doi.org/10.3749/canmin.48.2.351

Peucat J.J., Ruffault P., Fritsch E., Bouhnick-le Coz M., Simonet C., Lasnier B. (2007) Ga/Mg ratio as a new geochemical tool to differentiate magmatic from metamorphic blue sapphires. *Lithos*, Vol. 98, Nos. 1–4, pp. 261–274, http://dx.doi.org/10.1016/j.lithos.2007.05.001

Poitrasson F., Chenery S., Shepherd T.J. (2000) Electron microprobe

and LA-ICP-MS study of monazite hydrothermal alteration: Implications for U-Th-Pb geochronology and nuclear ceramics. *Geochimica et Cosmochimica Acta*, Vol. 64, No. 19, pp. 3283–3297, http://dx.doi.org/10.1016/S0016-7037(00)00433-6

Pratt J.H. (1906) *Corundum and Its Occurrence and Distribution in the United States*. U.S. Geological Survey, Bulletin 269, 175 pp.

Saeseaw S., Wang W., Scarratt K., Emmett J.L., Douthit T.R. (2009) Distinguishing heated spinels from unheated natural spinels and from synthetic spinels – a short review of on-going research. http://www.gia.edu/gia-news-research-NR32209A, 13 pp.

Schmetzer K., Schwarz D. (2005) A microscopy-based screening system to identify natural and treated sapphires in the yellow to reddish-orange colour range. *Journal of Gemmology*, Vol. 29, No. 7/8, pp. 407–449.

Schulze D.J. (2003) A classification scheme for mantle-derived garnets in kimberlite: A tool for investigating the mantle and exploring for diamonds. *Lithos*, Vol. 71, No. 2/4, pp. 195–213, http://dx.doi.org/10.1016/S0024-4937(03)00113-0

Schwieger R. (1990) Diagnostic features and heat treatment of Kashmir sapphires. *G&G*, Vol. 26, No. 4, pp. 267–280, http://dx.doi.org/10.5741/GEMS.26.4.267

Seifert A.V., Hyršl J. (1999) Sapphire and garnet from Kalalani, Tanga Province, Tanzania. *G&G*, Vol. 35, No. 2, pp. 108–120, http://dx.doi.org/10.5741/GEMS.35.2.108

Simonet C., Fritsch E., Lasnier B. (2008) A classification of gem corundum deposits aimed towards gem exploration. *Ore Geology Reviews*, Vol. 34, Nos. 1–2, pp. 127–133, http://dx.doi.org/10.1016/j.oregeorev.2007.09.002

Smith C. (2010) Inside sapphires. *Rapaport Diamond Report*, Vol. 33, No. 7, pp. 123–132.

Solesbury F. (1967) Gem corundum pegmatites in NE Tanganyika. *Economic Geology*, Vol. 62, No. 7, pp. 983–991, http://dx.doi.org/10.2113/gsecongeo.62.7.983

Sutherland F.L., Schwarz D., Jobbins E.A., Coenraads R.R., Webb G. (1998) Distinctive gem corundum suites from discrete basalt fields: a comparative study of Barrington, Australia, and West Pailin, Cambodia, gemfields. *Journal of Gemmology*, Vol. 26, No. 2, pp. 65–85.

Sutherland F.L., Duroc-Danner M., Meffre S. (2008) Age and origin of gem corundum and zircon megacrysts from the Mercaderes-Rio Mayo area, South-west Colombia, South America. *Ore Geology Reviews*, Vol. 34, pp. 155–168, http://dx.doi.org/10.1016/j.oregeorev.2008.01.004

Sutherland F.L., Abduriyim A. (2009) Geographic typing of gem corundum: a test case from Australia. *Journal of Gemmology*, Vol. 31, No. 5–6, pp. 203–210.

Sutherland F.L., Zaw K., Meffre S., Giuliani G., Fallick A.E., Graham I.T., Webb G.B. (2009) Gem corundum megacrysts from East Australian basalt fields: trace elements, O isotopes and origins. *Australian Journal of Earth Sciences*, Vol. 56, No. 7, pp. 1003–1020, http://dx.doi.org/10.1080/08120090903112109.

Wang A., Kuebler K.E. Bradley L., Haskin L.A. (2004) Raman spectroscopy of Fe-Ti-Cr-oxides, case study: Martian meteorite EETA 79001. *American Mineralogist*, Vol. 89, Nos. 5–6, pp. 665–680.

Whalen J.B., Currie K.L., Chappell B.W. (1987) A-type granites: geochemical characteristics, discrimination and petrogenesis. *Contributions to Mineralogy and Petrology*, Vol. 95, No. 4, pp. 407–419, http://dx.doi.org/10.1007/BF00402202

Williams T.J., Walters L. (2004) Mineral inclusions in alluvial sapphires from Browns Gulch, southwestern Montana; Implications for the origin of Montana alluvial sapphires. *Geological Society of America, Abstracts with Programs*, Vol. 36, No. 5, p. 225.

Zaw K., Sutherland F.L., Dellapasqua F., Ryan C.G., Yui T.F., Mernagh T.P., Duncan D. (2006) Contrasts in gem corundum characteristics, eastern Australian basaltic fields: trace elements, fluid/melt inclusions and oxygen isotopes. *Mineralogical Magazine*, Vol. 70, No. 6, pp. 669–687, http://dx.doi.org/10.1180/0026461067060356